Structural analysis and electrochemical properties of cobalt-doped $Sr_{0.9}Ce_{0.1}MnO_{3-\delta}$ cathode for IT-SOFCs

Jiseung Ryu
Department of Materials Science and Engineering, Pusan National University, Busan 609-735, Korea
Ryan O'Hayre
Metallurgical and Materials Engineering, Colorado School of Mines, Golden, Colorado 80401, USA
Heesoo Lee[a)]
Department of Materials Science and Engineering, Pusan National University, Busan 609-735, Korea

(Received 15 May 2014; accepted 2 October 2014)

Cobalt was doped into the Ce-doped $SrMnO_3$ system to enhance the low ionic conductivity of Ce-doped $SrMnO_3$ (SCM) for solid oxide fuel cell cathode application. Structural and conductivity changes as a function of the Co content were investigated. $Sr_{0.9}Ce_{0.1}Mn_{1-x}Co_xO_{3-\delta}$ (SCMCo, $x = 0.1$, 0.2, 0.3) cathode materials were synthesized by an EDTA citrate complexing process, which yielded a single perovskite structure, and the lattice volume was expanded by substituting Ce and Co ions. The increased lattice volume was attributed to a decrease in the valence state of the manganese and cobalt and an increase in the oxygen vacancy concentration. An increase in the concentration of oxygen vacancies with increasing Co content was identified by thermogravimetric analysis. The electrical conductivity decreased with increasing Co content, which was attributed to an increase in the activation energy for polaron hopping. Although the electrical conductivity was decreased by cobalt-doping, the polarization resistance of SCMCo also decreased significantly (from 5.611 to 1.171 Ω cm^2 at 800 °C). The decreased polarization resistance is attributed to enhanced oxygen-ion transfer kinetics with cobalt-doping. We conclude that cobalt substitution leads to enhancement in the electrochemical properties of the cathode due to an increase in oxygen vacancy concentration.

I. INTRODUCTION

Ce-doped $SrMnO_3$ (SCM) has received attention as a cathode material for intermediate temperature (600–800 °C) solid oxide fuel cells (SOFCs), because of its similar thermal expansion coefficient to ceria-based electrolytes as well as its high electrical conductivity (over 300 S cm^{-1} at 800 °C).[1–3] However, it is reported that SCM has low oxygen ion conductivity at intermediate temperatures.[1,4] We have previously used x-ray absorption spectroscopy to show that the insufficient oxygen ion conductivity in this material can be primarily attributed to a decrease in oxygen vacancy concentration with increasing Ce doping due to the strong hybridization between the Ce 4*f* and O 2*p* orbitals.[5]

It is well known that oxygen ion transfer in cathode materials with perovskite structures can be enhanced by oxygen vacancy formation through the heterovalent substitution of transition metal cations.[6–8] Among these, cobalt-doped mixed ionic and electronic conductors (MIECs) have received great attention. Rao et al.[9] investigated $BaZr_{1-x}Co_xO_{3-\delta}$ (BZC, $x = 0.1$, 0.2, 0.3, 0.4, and 0.5) as a cathode material for reversible solid oxide cells. They suggested that BZC maintains the perovskite structure for $x \leq 0.4$, and that both the electronic and the ionic conductivity increase with increasing cobalt addition up to $x = 0.4$. Trofimenko and Ullmann reported that oxygen ion transfer was enhanced by the creation of oxygen vacancies induced by Co ions in the MIEC $Sr_{1-a}Ce_aFe_{1-b}Co_bO_3$ ($a = 0$–0.4, $b = 0$–1.0), and that the resulting ionic conductivity was higher than that of a Gd-doped ceria electrolyte.[10] By analogy, it can be expected that Co-doping might also improve ionic conductivity in SCM, which can be expressed in Kröger–Vink notation as

$$\frac{1}{2}Co_2O_3 + \frac{1}{2}O_{2(g)} \underset{SrMnO_3}{\longrightarrow} Sr_{Sr^{2+}}^{\times} + Co_{Mn^{4+}}^{'} + \frac{1}{2}V_O^{\cdot\cdot} + \frac{5}{2}O_o^{\times} \quad .$$

To investigate this possibility, in this work we synthesize a series of Co-doped $Sr_{0.9}Ce_{0.1}MnO_3$ ($Sr_{0.9}Ce_{0.1}Mn_{1-x}Co_xO_{3-\delta}$, SCMCo) powders and examine the changes in conductivity as a function of Co content in the context of oxygen vacancy formation. The $Sr_{0.9}Ce_{0.1}MnO_3$ is selected as the base composition because it has a lower polarization and an acceptable electrical

a)Address all correspondence to this author.
e-mail: heesoo@pusan.ac.kr
DOI: 10.1557/jmr.2014.306

 © Materials Research Society 2014

https://doi.org/10.1557/jmr.2014.306 Published online by Cambridge University Press

conductivity within a series of $Sr_{1-x}Ce_xMnO_3$ (x = 0.1, 0.2, 0.3).[4] We focus on the crystal structural and conductivity changes, and apply 4-probe DC measurement to investigate the electrical conductivity of bar samples, and impedance measurement to investigate the electrochemical response of SCMCo/SDC/SCMCo, symmetric cathodes, respectively.

II. EXPERIMENTAL

A. Powder synthesis and sample preparation

All of the $Sr_{0.9}Ce_{0.1}Mn_{1-x}Co_xO_{3-\delta}$ (x = 0.1, 0.2, and 0.3) powders were synthesized using an EDTA citrate complexing process (ECCP). The necessary stoichiometric amount of $Sr(NO_3)_2$ (Sigma-Aldrich, ≥99%), $Ce(NO_3)_3{\cdot}6H_2O$ (Alfa Aesar, ≥99.5%), $Mn(CH_3COO)_2{\cdot}4H_2O$ (Sigma-Aldrich, ≥99%), and $Co(NO_3)_2{\cdot}6H_2O$ (Junsei, ≥98%) metal precursors were weighed and dissolved in distilled water. An NH_3-EDTA buffer solution was prepared by mixing ethylenediaminetetraacetic acid powder (EDTA acid powder, Alfa Aesar) and a 1N NH_4OH solution. The NH_3-EDTA and citric acid (Samchun chemical, ≥99.5%) for chelation were gradually added to the mixed metal solution to reach total metal ion : EDTA : citric acid molar ratio of 1:1:2. NH_4OH was dropped to adjust the pH value of the solution to approximately 8 during the water evaporation step. Under stirring and heating at 80 °C, a viscous gel was obtained, which was subsequently solidified by baking in an oven at 750 °C for 4 h. The calcined powders were ground and pressed into pellets and bar type samples under uniaxial pressure. The green samples were sintered in air at 1350 °C for 3 h to achieve dense ceramic bodies for electrical conductivity measurements. Relative densities of all sintered samples, as measured by Archimedes' method, were determined to be between 96–97%. Table I shows the abbreviations of the $Sr_{0.9}Ce_{0.1}Mn_{1-x}Co_xO_{3-\delta}$ cathodes according to the Co content.

B. Cell preparation

Symmetric cells were prepared to investigate the electrochemical properties of the SCMCo10, SCMCo20, and SCMCo30 cathodes supported on $Ce_{0.8}Sm_{0.2}O_2$ (SDC, Fuel Cell Materials) electrolyte pellets. The 15 mm diameter and 1.5 mm thick SDC electrolyte pellets were sintered at 1500 °C for 5 h. The SCMCo powders, which were prepared by ball-milling in ethanol after crushing the sintered pellet, were mixed with a binder prepared from α-terpineol and ethyl-cellulose to form cathode pastes. The detailed procedure for the cell preparation is given in a preceding paper.[4]

C. Characterization

X-ray diffraction patterns of the sintered powders were recorded at room temperature using a step scan procedure (0.02°/2θ step, 5 s/step) in the 2θ range of 10–150° (Ultima IV, Rigaku). Rietveld refinement based on the x-ray diffraction patterns was conducted using the Fullprof software package. In the final run stage, five background coefficients, scale factors, and unit cell parameters were refined from the collected XRD scans. Site occupancies were fixed according to the results of the chemical analysis. The weight loss of the samples was examined by thermogravimetric (TG) analysis using a NETZSCH STA 409 thermal gravity analyzer (Germany) under flowing air atmosphere at the rate of 10 mL min^{-1}. Twenty-milligram samples were used for this analysis.

Electrical conductivity (σ) was measured through 4 probe DC measurement from 500 to 1000 °C in air using Pt wires. Electric current was supplied by a Keithley 2400 current source, and the voltage was measured using an Agilent 34401A digital multimeter (Santa Clara, CA).

Impedance measurements were carried out using an IviumStat (Ivium, Netherlands) instrument over a frequency range from 10^6 to 0.01 Hz with a 10 mV excitation voltage at operating temperatures of 650, 750, and 800 °C in air. The impedance measurements were acquired under an open circuit condition. The electrochemical impedance spectra (EIS) results were multiplied by 0.5 to account for the two electrodes. The measured impedance data were plotted on the complex plane, and were fitted to an equivalent circuit using Zview software (Solartron Analytical).

III. RESULTS AND DISCUSSION

A. Structural characterization

Figure 1 shows the x-ray diffraction patterns and results of Rietveld refinement of the SCMCo10, SCMCo20, and SCMCo30 powders sintered at 1350 °C for 4 h. The refined lattice parameters, the weighted R factor (R_{wp}), the expected R factor (R_{exp}), and the goodness of fit (χ^2) are also presented in Table II. All cobalt-doped SCM samples presented perovskite peaks, which reveal the I4/mmm tetragonal space group. It is reported that A-site doping elements can induce changes to the electrovalence of the B-site cations in the SCM system due to charge compensation effects.[11,12] It was also investigated that the expansion in a unit cell volume increases due to a progressive increase in the oxygen vacancy concentration.[13] Therefore, we support that the substitution of Ce ions and Co ions on the A-site and B-site, respectively, of SCMCo induces partial reduction of manganese and cobalt on the B-site and an increase in the oxygen vacancy concentration, which would contribute to the observed lattice expansion.

Figure 2 shows the TG curves of SCM and SCMCo samples in air, which we use to investigate the oxygen vacancy concentration due to Co doping. For all SCMCo samples, the weight loss increases steadily with increasing temperature. This weight loss is associated

https://doi.org/10.1557/jmr.2014.306 Published online by Cambridge University Press

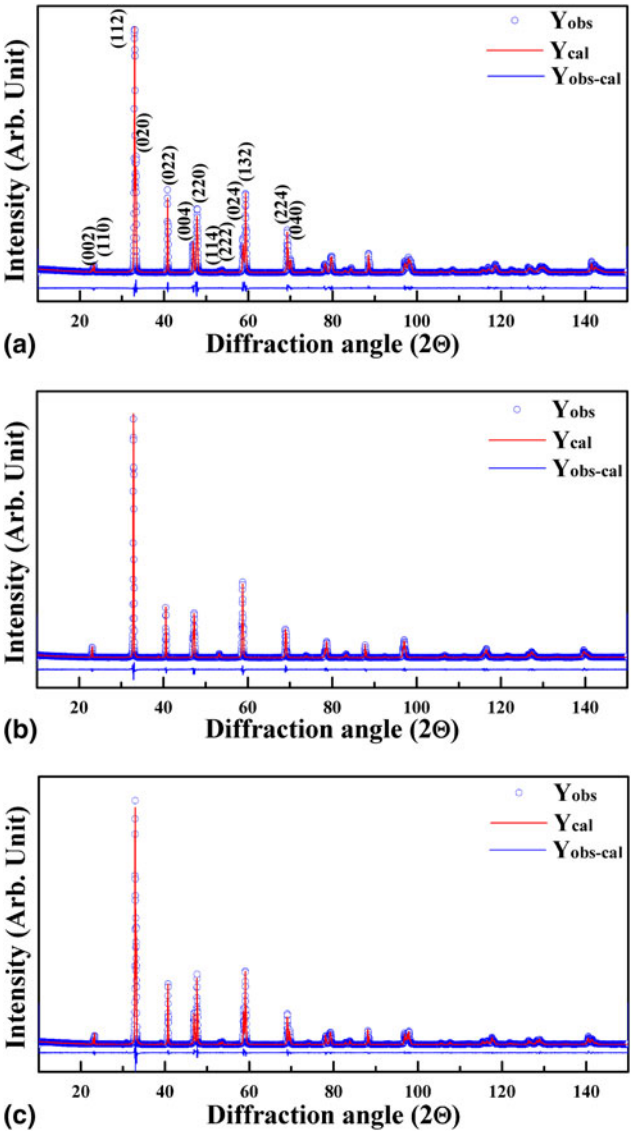


FIG. 1. Observed (open symbols) and refined (solid line) x-ray diffraction patterns of Co-doped $Sr_{0.9}Ce_{0.1}MnO_{3-\delta}$: (a) SCMCo10, (b) SCMCo20, and (c) SCMCo30. The difference residuals between the observed and calculated intensities are also provided.

TABLE I. Composition and abbreviation of $Sr_{0.9}Ce_{0.1}Mn_{1-x}Co_xO_{3-\delta}$.

Co content	Composition	Abbreviation
$x = 0$	$Sr_{0.9}Ce_{0.1}MnO_3$	SCM
$x = 0.1$	$Sr_{0.9}Ce_{0.1}Mn_{0.9}Co_{0.1}O_{3-\delta}$	SCMCo10
$x = 0.2$	$Sr_{0.9}Ce_{0.1}Mn_{0.8}Co_{0.2}O_{3-\delta}$	SCMCo20
$x = 0.3$	$Sr_{0.9}Ce_{0.1}Mn_{0.7}Co_{0.3}O_{3-\delta}$	SCMCo30

with loss of oxygen from the crystal lattice and the consequent formation of oxygen vacancies, commensurate with the reduction of the B-site transition metal ions.[14] The formation of oxygen vacancies in SCMCo can be expressed in the Kröger–Vink notation as

TABLE II. Structural parameters of $Sr_{0.9}Ce_{0.1}Mn_{1-x}Co_xO_{3-\delta}$ sintered at 1350 °C after Rietveld refinements of the room temperature XRD data.

	Composition		
Parameters	SCMCo10	SCMCo20	SCMCo30
$a = b$ [Å]	5.402(4)	5.412(0)	5.403(2)
c [Å]	7.644(0)	7.656(4)	7.721(1)
Volume [Å^3]	223.097	224.254	225.414
Structure	I4/mmm	I4/mmm	I4/mmm
R_{wp} [%]	16.8	15.4	14.8
R_{exp} [%]	8.12	7.08	8.12
χ^2	4.28(1)	4.73(1)	3.32(2)

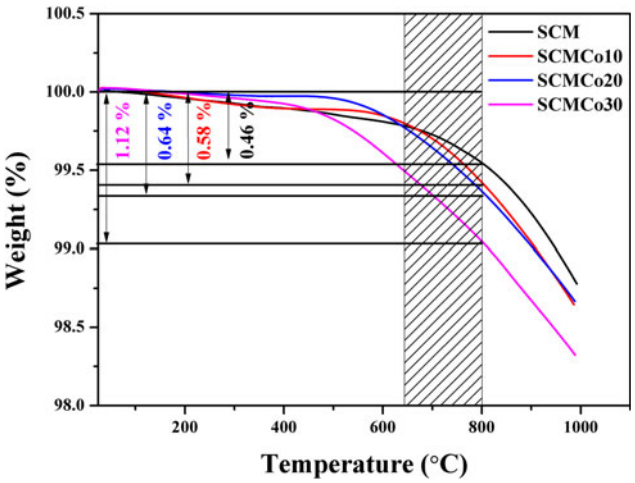


FIG. 2. TG curves of the SCM and Co-doped SCM in air.

$$2Mn^{\cdot}_{Mn^{4+}} + O^{\times}_{O} \rightarrow 2Mn^{\times}_{Mn^{4+}} + V^{\cdot\cdot}_{O} + \frac{1}{2}O_2 \quad ,$$

$$2Co^{\cdot}_{Co^{4+}} + O^{\times}_{O} \rightarrow 2Co^{\times}_{Co^{4+}} + V^{\cdot\cdot}_{O} + \frac{1}{2}O_2 \quad .$$

The weight losses of SCMCo compositions were higher than that of SCM (0.46%) over 650 °C, which indicated that the concentration of oxygen vacancy was increased by the substitution of Co for Mn. Above 650 °C, the weight loss of the SCMCo composition also increases with increasing Co content, suggesting that the oxygen vacancy concentration in SCMCo increases with increasing Co content.

B. Electrical conductivity

Figure 3 provides the Arrhenius plots of the measured electrical conductivity (S cm^{-1}) of the SCM and SCMCo samples sintered at 1350 °C as a function of temperature. Co-doped SCM presents lower electrical conductivity than SCM and the conductivity gradually decreases with increasing Co content. For example, the

https://doi.org/10.1557/jmr.2014.306 Published online by Cambridge University Press

conductivity of the SCMCo10 sample was 108 S cm^{-1} at 750 °C while the conductivity of SCMCo30 was 103 S cm^{-1} at 750 °C. Nevertheless, both of these values are considered acceptable (preferably more than 100 S cm^{-1})[15,16] for SOFC cathodes.

All of the SCM and SCMCo specimens exhibited an Arrhenius temperature dependence with modest ($0.03 < E_a < 0.14$ eV activation energies) over a wide range of temperatures. The results are characteristic of a small polaron hopping mechanism, which is frequently observed in the perovskite structures along the transition metal-oxygen-transition metal chains.[17] The increase in activation energy (E_a) for electron conduction with the addition of Co ions suggests that Co substitution increases the barrier for polaron hopping.[18]

C. Polarization resistance

Figure 4 shows the EIS for symmetric cells of the SCM and SCMCo cathodes on the SDC electrolyte at 650 and 750 °C. The inductive response, with respect to the Pt wire connection and the instrumentation, was subtracted from the impedance spectra. The difference between the low- and high-frequency intercepts of the semicircular impedance arc can be used to determine the polarization resistance of the cathode (R_p). R_p represents the overall cathodic resistance, including oxygen reduction, oxygen surface/bulk diffusion, and gas-phase oxygen diffusion.

The R_p values decrease with increasing temperature, due to the increase in the charge carrier transfer rate (for both electron and oxygen ions) at higher temperatures. The R_p values of the Co-doped SCM cathodes were also significantly lower than that of the SCM cathode, with the lowest R_p obtained for the cathode with the highest Co content. These results suggest that Co-substitution enhances either the oxygen reduction (charge transfer) process and/or the oxygen surface/bulk diffusion process within the cathode, despite the lower electrical conductivity of Co-doped SCM.

Figure 5 shows the EIS for symmetric cells of the SCMCo cathodes at 800 °C fitted by an equivalent circuit. The impedance spectra are evaluated by fitting impedance data with an equivalent circuit that consists of an ohmic resistance (R_{ohm}) in series with an inductance (L) and a series combination of two parallel resistance/constant phase elements (R_1Q_1 and R_2Q_2). The calculated resistance values associated with the high- and low-frequency arcs (R_1 and R_2), as well as the polarization resistance ($R_p = R_1 + R_2$), are tabulated in Table III. A good agreement is observed between the observed data and the fitted data with equivalent circuit, which indicates that the equivalent circuit is a reasonable approximation.

The R_p value decreases with an increase in Co content, and SCMCo30 shows the lowest R_p value (1.171 Ω cm^2 at 800 °C) among the compositions examined. The decrease in R_p as a function of the Co

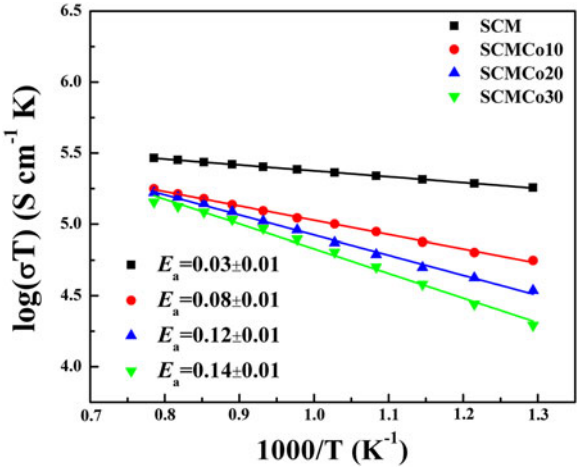


FIG. 3. Arrhenius plots and activation energies for the electrical conductivity of SCM and Co-doped SCM.

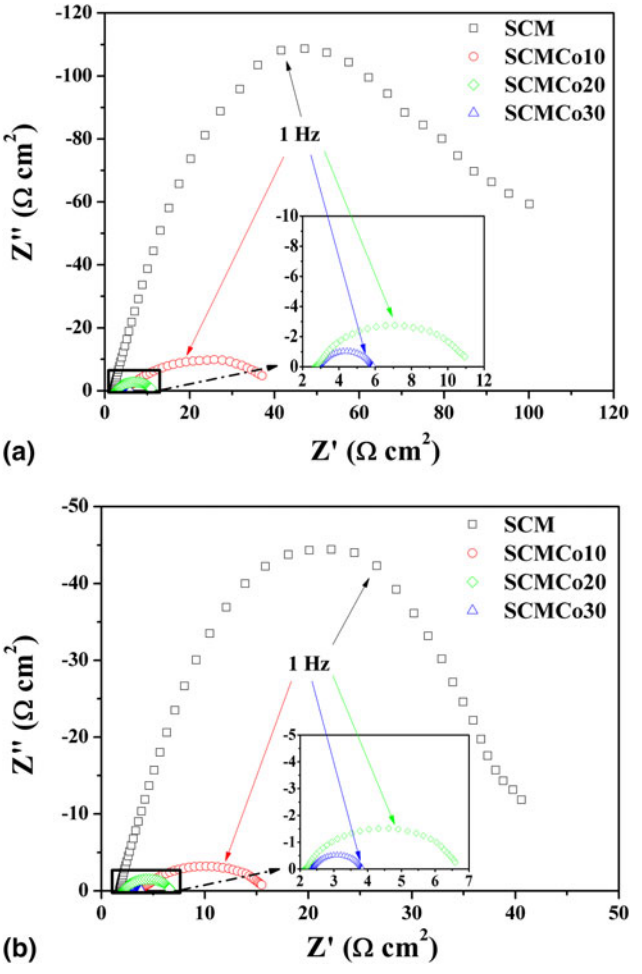


FIG. 4. Comparison of impedance spectra for the SCM and SCMCo symmetric cells on the SDC electrolyte in air at zero DC bias: (a) 650 °C and (b) 750 °C.

https://doi.org/10.1557/jmr.2014.306 Published online by Cambridge University Press

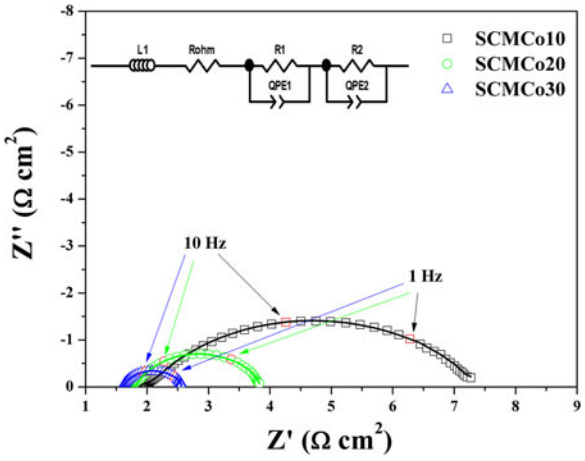


FIG. 5. Impedance spectra and equivalent circuits of the symmetric cells with the SCMCo cathodes on the SDC electrolyte obtained in air at 800 °C at zero DC bias.

TABLE III. Impedance spectra fitting results for symmetric cells of SCMCo cathodes measured at 800 °C.

Composition	SCMCo10	SCMCo20	SCMCo30
L ($\times 10^{-6}$ H cm^2)	0.588	1.214	1.168
R_{ohm} (Ω cm^2)	1.849	1.607	1.410
R_1 (Ω cm^2)	0.237	0.201	0.197
QPE1-T ($\times 10^{-6}$ F cm^{-2})	3.648	2.472	2.170
QPE1-P	0.781	1.188	1.268
R_2 (Ω cm^2)	5.374	2.066	0.971
QPE2-T ($\times 10^{-3}$ F cm^{-2})	0.151	3.273	5.064
QPE2-P	0.648	0.762	0.783
R_p (R_1 + R_2) (Ω cm^2)	5.611	2.267	1.171

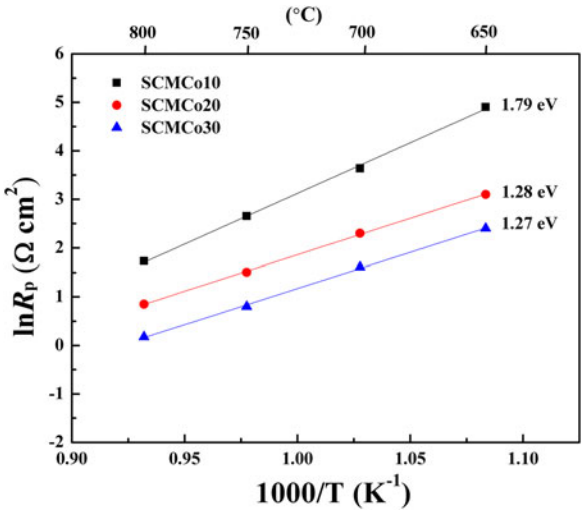


FIG. 6. Polarization resistances of the SCMCo cathodes on the SDC electrolyte in air.

content is due to both a decrease in R_1 and R_2. R_1 is commonly associated with charge transfer processes, which include oxygen ion diffusion in the bulk of cathode, while R_2 is commonly attributed to surface and gas-phase processes, including the adsorption–desorption process of oxygen, oxygen diffusion at the gas/cathode interface, and surface diffusion of intermediate oxygen species.[19,20] Bulk and surface diffusion of oxygen ions in cathode materials can be improved by the formation of oxygen vacancies, thereby helping explain the decrease in both R_1 and R_2 in the SCMCo system with increasing Co composition.

The polarization resistances in Fig. 6 as a function of temperature show a single slope, which indicates that the same reaction mechanisms likely control the overall electrode reaction across the measured temperature range for each cathode. The activation energy (E_a) for the R_p of SCMCo10 is 0.78 eV. In contrast, the E_a of the SCMCo20 and SCMCo30 compositions is appreciably reduced to 0.46–0.47 eV. The marked decrease in both R_p and E_a for the 20 and 30 mol% Co-doped compositions suggests an increase in the oxygen ionic conductivity in SCMCo cathode materials.

IV. CONCLUSION

$Sr_{0.9}Ce_{0.1}Mn_{1-x}Co_xO_{3-\delta}$ (x = 0.1, 0.2, and 0.3) powders synthesized by an ECCP have a single perovskite structure, and the lattice volume, determined by Rietveld refinement, expands with an increase in the Co content. The reduction of manganese and cobalt ions and an increase in the oxygen vacancy concentration would be consistent with the observed volume expansion of crystal structure. We confirm that the weight loss in the SCMCo system increases with increasing Co content above 600 °C, which provides further evidence of increasing oxygen vacancy concentration with Co substitution. Cobalt-doping in SCM reduces the electrical conductivity, and the conductivity values of SCMCo10, SCMCo20, and SCMCo30 were 108, 106, and 103 S cm^{-1} at 750 °C, respectively. Despite the small decrease in electrical conductivity, the cathodic polarization resistance (R_p) values of Co-doped compositions are significantly lower than that of the $Sr_{0.9}Ce_{0.1}MnO_{3-\delta}$. The SCMCo30, especially, showed the lowest R_p value, 1.171 cm^2 at 800 °C. These results show that the ORR kinetics of SCMCo are substantially enhanced in comparison with that of SCM, which associated with the increase in oxygen-ion transfer. We reason that the enhanced electrochemical properties of SCMCo may be attributed to an increase in oxygen vacancy concentration, caused by charge compensation effects induced by the doping of Co ions on the B-site of the SCM system.

ACKNOWLEDGMENTS

This work was supported by the National Research Foundation of Korea (NRF) grant funded by the Korean government (MSIP) through GCRC-SOP

https://doi.org/10.1557/jmr.2014.306 Published online by Cambridge University Press

(No. 2011-0030013). We are also especially appreciative to Ms. Mary Van Tyne for her language editing of the manuscript.

REFERENCES

1. S. Hashimoto and H. Iwahara: Structural, thermal and electrical properties of Ce-doped $SrMnO_3$. *J. Electroceram.* **4**, 225 (2000).
2. S. Hashimoto and H. Iwahara: Study on the structural and electrical properties of $Sr_{1-x}Ce_xO_{3-\alpha}$ (x = 0.1, 0.3) perovskite oxide. *Mater. Res. Bull.* **35**, 2253 (2000).
3. K.J. Lee and E. Iguchi: Electronic properties of $SrMnO_3$. *J. Solid State Chem.* **114**, 242 (1995).
4. C. Jeong, J. Ryu, T. Noh, Y-N. Kim, and H. Lee: Structural analysis and electrode performance of Ce doped $SrMnO_3$ synthesized by EDTA citrate complexing process. *Adv. Appl. Ceram.* **112**, 494 (2013).
5. J. Ryu, R. O'Hayre, and H. Lee: Polarization resistance and composite cathode of Ce doped $SrMnO_3$ system for intermediate temperature solid oxide fuel cells. *Solid State Ionics* **260**, 60 (2014).
6. K. Huang, H. Lee, and J. Goodenough: Sr- and Ni-doped $LaCoO_3$ and $LaFeO_3$ perovskites new cathode materials for solid oxide fuel cells. *J. Electrochem. Soc.* **145**(9), 3220 (1998).
7. F. Chen and M. Liu: Study of transition metal oxide doped $LaGaO_3$ as electrode materials for LSGM-based solid oxide fuel cells. *J. Solid State Electrochem.* **3**, 7 (1998).
8. T. Noh, J. Ryu, J. Kim, Y-N. Kim, and H. Lee: Structural and impedance analysis of copper doped LSM cathode for IT-SOFCs. *J. Alloys Compd.* **557**, 196 (2013).
9. Y. Rao, S. Zhong, F. He, Z. Wang, R. Peng, and Y. Lu: Cobalt-doped $BaZrO_3$: A single phase air electrode material for reversible solid oxide cells. *Int. J. Hydrogen Energy* **37**(17), 12522 (2012).
10. N.E. Trofimenko and H. Ullmann: Oxygen stoichiometry and mixed ionic-electronic conductivity of $Sr_{1-a}Ce_aFe_{1-b}Co_bO_{3-x}$ perovskite-type oxides. *J. Eur. Ceram. Soc.* **20**, 1241 (2000).
11. P. Mandal, A. Hassen, and A. Loidl: Effect of Ce doping on structural, magnetic, and transport properties of SrMnO3 perovskite. *Phys. Rev. B* **69**(22), (2004).
12. A. Sundaresan, J.L. Tholence, A. Maignan, C. Martin, M. Hervieu, B. Raveau, and E. Suard: Jahn-Teller distortion and magnetoresistance in electron doped $Sr_{1-x}Ce_xMnO_3$ (x = 0.1, 0.2, 0.3 and 0.4). *Eur. Phys. J. B* **14**, 431 (2000).
13. A. Fossdal, M. Menon, I. Waernhus, K. Wiik, M-A. Einarsrud, and T. Grande: Crystal structure and thermal expansion of $La_{1-x}Sr_xFeO_{3-\delta}$ materials. *J. Am. Ceram. Soc.* **87**, 1952 (2004).
14. L. Ge, Z. Zhu, Z. Shao, S. Wang, and S. Liu: Effects of preparation methods on the oxygen nonstoichiometry, B-site cation valences and catalytic efficiency of perovskite $La_{0.6}Sr_{0.4}Co_{0.2}Fe_{0.8}O_{3-\delta}$. *Ceram. Int.* **35**(8), 3201 (2009).
15. C. Sun, R. Hui, and J. Roller: Cathode materials for solid oxide fuel cells: A review. *J. Solid State Electrochem.* **14**(7), 1125 (2009).
16. A. Aguadero, C.D.L. Calle, J.A. Alonso, M.J. Escudero, M.T. Fernandez-Diaz, and L. Daza: Structural and electrical characterization of the novel $SrCo_{0.9}Sb_{0.1}O_{3-\delta}$ perovskite: Evaluation as a solid oxide fuel cell cathode material. *Chem. Mater.* **19**, 6437 (2007).
17. C. Zener: Interaction between the d-shells in the transition metals. II. Ferromagnetic compounds of manganese with perovskite structure. *Phys. Rev.* **82**(3), 403 (1951).
18. S. Pal, A. Banerjee, E. Rozenberg, and B.K. Chaudhuri: Polaron hopping conduction and thermoelectric power in $LaMnO_{3+\delta}$. *J. Appl. Phys.* **89**(9), 4955 (2001).
19. E.P. Murray, M.J. Sever, and S.A. Barnett: Electrochemical performance of (La,Sr)(Co,Fe)O_3-(Ce,Gd)O_3 composite cathodes. *Solid State Ionics* **148**, 27 (2002).
20. F. Qiang, K. Sun, N. Zhang, X.D. Zhu, S.D. Le, and D.R. Zhou: Characterization of electrical properties of GDC doped A-site deficient LSCF based composite cathode using impedance spectroscopy. *J. Power Sources* **168**(2), 338 (2007).

https://doi.org/10.1557/jmr.2014.306 Published online by Cambridge University Press